'93 한국자동제어학술회의논문집 (1993.10.20~22)

유연한 조작기의 끝점위치 및 접촉력 제어

최 병 오
한국기계연구원

End Point and Contact Force Control of a Flexible Manipulator

Byung-Oh Choi
Korea Institute of Machinery & Metals

ABSTRACT

In this paper, control of a planar two-link structurally flexible robotic manipulator executing unconstrained and constrained maneuvers is considered. The dynamic model, which is obtained by using the extended Hamilton's principle and the Galerkin criterion, includes the impact force generated during the transition from unconstrained to constrained segment of the robotic task. A method is presented to obtain the linearized equations of motion in Cartesian space for use in designing the control system. The linear quadratic Gaussian with loop transfer recovery (LQG/LTR) design methodology is exploited to design a robust feedback control system that can handle modeling errors and sensor noise, and operate on Cartesian space trajectory errors. The LQG/LTR compensator together with a feedforward loop is used to control the flexible manipulator. Simulated results are presented for a numerical example.

1. INTRODUCTION

The task description of robotic manipulators varies considerably ranging from point-to-point control for a pick-and-place task, to continuous path control for painting, seam welding, and inspection, to force control for deburring, grinding, and part mating. Robotic maneuvers can be classified into two categories: unconstrained and constrained maneuvers. An unconstrained maneuver is where the end-point of the robotic manipulator moves in free space. The control objective in this case is to control the position of the end-point. A constrained maneuver is where the end-point of the robotic manipulator exerts a specified force on the environment as it moves along a specified path. Here, the control objective is to simultaneously control the force exerted by the end-point in a direction normal to the environment and the position of the end-point in a direction tangential to the environment.

In the past, a vast number of theoretical and some experimental studies have been conducted on unconstrained maneuvers of single- and multi-link structurally flexible robotic manipulators. However , only a few studies have considered constrained motion, and combined unconstrained and constrained motion of flexible robotic manipulators. Maples [1] addressed the problem of controlling contact force at one end of a very flexible arm by precisely controlling the torque exerted at the other end. Maples presented experimental results showing that good closed-loop force control can be obtained using end-point feedback. Results include a maneuver in which the flexible arm is slewed rapidly to contact a moving target and then switching from end-point position control to end-point force control. Tilley and Cannon [2] found that significant improvement in performance can be obtained by using a fast micro-manipulator at the end of the very flexible manipulator. The fast wrist makes it possible to control the tip velocity to be low and independent of the main arm at the time of contact so that the impulsive forces generated during touchdown are reduced. Encouraged by their results with the one-degree-of-freedom wrist, Tilley, *et al.* [3] presented a two-degree-of-freedom wrist is expected to have better performance. The improved performance with a micro-manipulator at the end of a flexible beam is attained at the expense of increased cost due to the additional hardware, however.

Fan and Castelazo [4] considered the problem of controlling the force exerted by a single flexible robot arm, which is assumed to be in contact with a rigid environment. They showed that by using a PID controller together with an optimal controller, good transient response without any steady-state error could be obtained. Matsuno, *et al.* [5] studied hybrid position/force control of a two-link planar manipulator with one flexible link. The contact force between the end-point of the manipulator and the constraint surface was incorporated into the Hamilton's principle using the method of Lagrange multipliers. a nonlinear decoupling controller was presented for the equations of motions simplified for the quasi-static case. Experimental results were presented for a maneuver where the desired tip speed and contact force were 0.014 m/s and 19.6 N, respectively.

Chiou and Shahinpoor [6,7] studied the effects of joint and link flexibilities on the dynamic stability of a force controlled two-link manipulator. The closed-loop equations were obtained using stiffness control, damping control and hybrid position/force control methods. The results show different stability characteristics depending on the control method employed, and whether joint or link flexibility is considered. In another study, Chiou and Shahinpoor [8] presented computer simulated and experimental results on the dynamic stability of a single-link force controlled manipulator. The computer

simulated results show that the elastic modes can be excited by the force control action, which in turn can make the system unstable. In addition to this, experimental results show a delay of force actuation and occurrence of impact could be detrimental to the system dynamic stability. Similar conclusions were drawn by Eppinger and Seering [9]. They studied the effects of structural flexibility, sensor and work piece dynamics using a series of lumped parameter models.

Pfeiffer [10] and Richter and Pfeiffer [11] conducted experiments on the end-point position and contact force control of a two-link manipulator with three rigid degrees of freedom. The manipulator was considered to have both joint and link flexibility. The control scheme made use of feedforward and feedback torques. Static correction terms to compensate for joint and link deformations were included with the feedforward torques obtained by assuming the manipulator to be rigid. The feedback torques were obtained by using a PD controller for the joint position and a P (PI) controller for the link curvature. Richter and Pfeiffer have shown that strain gauges used to measure the link deflections can also be used to measure the force applied at the end-point. The results presented show that the force measured by strain gauges and a piezo sensor were comparable in accuracy.

The results presented in Refs.[1-11] are extremely useful in understanding the role of structural flexibility in force control. However, to be useful in industry, a thorough study of flexible manipulators with multiple degrees of freedom is necessary. Thus, force control with flexible manipulators is still an open issue and further investigation is required to design the next generation of high performance robotic manipulators.

Note that constrained problem is not new, a number of algorithms have been proposed for rigid manipulators. Stiffness control achieves force control by controlling the end-effector stiffness charateristics in the Cartesian space. Accommodation or damping control uses the measured force to modify the velocity command input. Hybrid position and force control uses two feedback loops to control force along position constrained directions and position along force constrained directions. The so-called selection matrices are used to identify which degrees of freedom in the task frame are to be position controlled and where are to be force controlled. The joint compliance method uses certain joint for position control and other remaining joints are used for force control Impedence control attempts to control position and force by adjusting the mechanical impedence of the end-effector. This method can be thought of as a generalization of stiffness and damping control. Other methods developed are hybrid impedence, dynamic force feedback, and external force control. A comparison of the various methods can be found in Ref. [12].

The LQG/LTR desigh methodology uses both frequency and time domain concepts. The performance requirement is specified in the low-frequecy range, while the stability-robustness requirement is specified in the high-frequency range. The minimum and maximum singular values of the loop transfer function matrix of the multi-input, multi-output (MIMO) system can be shaped to meet the requirements in frequency domain by picking the free design parameters appropriately. An attractive feature of the procedure is that the calculations to select the free design parameters in the filter and control gain matrices are performed in time domain. The technique of shaping the singular values is basically an extension of the classical single-input, single-output technique to MIMO systems. The LQG/LTR design methodology has been successully applied to a number of systems including a turoshaft engine coupled with a helicopter rotor system, a twin lift helicopter system, turbofan jet engines, roll attitude control of an unmanned aircraft, and submersible.

In this study, the problem of unconstrained and constrained motion control of high-speed, lightweight robotic manipulators in Cartesian space is considered. The objective is to design a control system for combined unconstrained and constrained maneuvers. The nonlinear integro-differential equations of motion are derived using the extended Hamilton's principle. Then using the Galerkin criterion, the partial differential equations are converted into a set of ordinary differential equations. The approach to solving the control problem is to use feedforward torques to maneuver the flexible manipulator along the nominal trajectory and feedback torques to minimize deviation from the nominal trajectory. The feedforward torques are obtained by solving the inverse dynamics problem for the rigid link manipulator. Linear quadradic Gaussian with loop transfer recovery compensators are designed to provide feedback torques. The design is based on the linearized dynamic model in Cartesian space obtained using a variational calculus technique. Computer simulated results are presented for an example planar two-link structurally flexible robotic manipulator to illustrate the effectiveness of the methodology.

2. MODEL FORMULATION

The equations of motion for a planar two-link structurally flexible robotic manipulator shown in Fig.1 can be derived in joint space as

$$M(Q)\ddot{Q}+KQ+N(Q,\dot{Q})=E\tau+J^T(Q)F \qquad (1)$$

where Q is the generalized coordinate vector, N is the vector containing nonlinear terms, τ is the input torque vector, F is the reaction force applied to the end-point by the environment, M, K, J, and E are the mass, stiffness, Jacobian, and control distribution matrices, respectively. The details of the nonlinear equations of motion can be found in Ref. [13]. By using a technique from variational calculus, Eq. (1) can be linearized about a nominal trajectory as

$$[M-(J^TF)_{\ddot{Q}}]^*\delta\ddot{Q}+[N_{\dot{Q}}-(J^TF)_{\dot{Q}}\delta\dot{Q} +[(M\ddot{Q})_Q+K+N_Q-(J^TF)_Q]^*\delta Q=E^*\delta\tau, \qquad (2)$$

where $[]^*$ denotes that the quantity is evaluated along the nominal trajectory, and subscript denotes partial derivative of the matrix/vector with respect to the su bscript.

The Cartesian position, velocity, and acceleration of the end-point can be written as

$$X=f(Q), \quad \dot{X}=J\dot{Q}, \quad \ddot{X}=J\ddot{Q}+\dot{J}\dot{Q}, \qquad (3a,b,c)$$

where J is the Jacobian. The first variation of Eqs. (3) can be obtained as

$$\delta X = J\,\delta Q, \qquad \delta \dot{X} = (J\dot{Q})_Q \delta Q + J\,\delta \dot{Q},$$
$$\delta \ddot{X} = (J\ddot{Q} + \dot{J}\dot{Q})_Q \delta Q + (J\dot{Q})_{\dot{Q}} \delta \dot{Q} + J\,\delta \ddot{Q}. \qquad (4a,b,c)$$

By augmenting the Cartesian position vector X with elements of the generalized coordinate vector Q corresponding to the link flexibility, Eqs. (4) can be rewritten as

$$\delta Q = J_a^{-1}\delta X_a \qquad \delta \dot{Q} = J_a^{-1}[\delta \dot{X}_a - (J_a\dot{Q})_Q J_a^{-1}\delta X_a],$$
$$\delta \ddot{Q} = J_a^{-1}[\delta \ddot{X}_a - (J_a\ddot{Q} + \dot{J}_a\dot{Q})_Q J_a^{-1}\delta X_a \qquad (5a,b,c)$$
$$-(J_a\dot{Q})_{\dot{Q}} J_a^{-1}[\delta \dot{X}_a - (J_a\dot{Q})_Q J_a^{-1}\delta X_a]],$$

where X_a is the augmented Cartesian position vector and J_a is the augmented Jacobian. Using Eqs. (2) and (5), and by modeling the force sensor which will be used to measure the force applied on the environment as a spring, a model in Cartesian space can be obtained in state-space form to design the LQG/LTR compensators as

$$\dot{Z}(t) = A(t)Z(t) + B(t)u(t),$$
$$Y(t) = CZ(t), \qquad (6a,b)$$

where the system matrices $A(t)$, $B(t)$, and C are appropriately defined. Equations (6) describe the behavior of the system around the nominal trajectory.

3. IMPACT MODEL

In general, collision occurs when the manipulator's end point makes contact with the environment because the relative velocity between the manipulator's end-point and the environment is nonzero. The jump discontinuity in the generalized velocity vector and the impulsive force at the contact point are of interest when collision occurs.

The collision will be assumed to occur for a very short period of time. Therefore, any changes in the generalized coordinate vector will be neglected. Applying the impulse-momentum principle yields

$$M\,\Delta\dot{Q} = \int_{t_0}^{t_0+\Delta t} J^T F\,dt, \qquad (7)$$

where $\Delta t \to 0$, $\Delta\dot{Q} = \dot{Q}(t_0+\Delta t) - \dot{Q}(t_0)$ is the jump discontinuity in the generalized velocity vector, and the time integral is the generalized impulsive force. Note that collision occurs when $X = X_e$ where X_e is the inertial position of the contact point on the environment. Therefore, the relative velocity between the manipulator's end-point and the environment (assumed to be stationary) is

$$\dot{X} = J\dot{Q}. \qquad (8)$$

Because the Jacobian is continuous, one can write

$$\dot{X}(t_0+\Delta t) - \dot{X}(t_0) = J\,\Delta\dot{Q}, \qquad (9)$$

which can be rewritten as

$$-(1+e)\dot{X}(t_0) = J\,\Delta\dot{Q}, \qquad (10)$$

where e is the coefficient of restitution. Combining Equations (7) and (10) yields

$$\int_{t_0}^{t_0+\Delta t} F dt = -(1+e)[JM^{-1}J^T]^{-1}\dot{X}(t_0), \qquad (11)$$

and combining Equations (7) and (11) yields

$$\Delta\dot{Q} = -(1+e)M^{-1}J^T[JM^{-1}J^T]^{-1}\dot{X}(t_0). \qquad (12)$$

Equations (11) and (12) can be used to obtain the impulsive force at the manipulator's end-point and the jump discontinuity in the generalized velocity vector when collision occurs.

4. CONTROL SCHEME AND LQG/LTR COMPENSATOR DESIGN

The control strategy to execute a specified maneuver efficiently is to apply feedforward and feedback torques. Therefore, the overall control input to the flexible manipulator is given by

$$U = \bar{u} + u, \qquad (13)$$

where $\bar{u}$ and u are the feedforward and feedback torques, respectively. A block diagram of the control system is shown in Fig. 2. The basic approach is to use feedforward torques to maneuver the flexible manipulator along the nominal trajectory and use feedback torques to minimize deviation from the nominal trajectory.

For a given manipulator task, the reference trajectory can be planned ahead of time. Therefore, the feedforward torques can be calculated without difficulty. In this study, the feedforward torques were obtained by solving the inverse dynamics problem with only rigid body terms in the equations of motion (1). The feedback control torques are obtained by designing LQG/LTR compensators using the linearized equations of motion in Cartesian space (6). Note that although the general control scheme is not new, designing LQG/LTR compensators to obtain feedback control torques has been only briefly investigated by Ward [14].

The linearized equations of motion in Cartesian space are time-varying. Therefore, LQG/LTR compensators are designed using the system model at set points along the desired trajectory. The performance specifications the LQG/LTR compensators have to meet are good command following, good disturbance rejection, insensitivity to sensor noise and unmodeled dynamics (stability - robustness), zero steady-state error to step command and disturbance inputs. Also, it is desirable to have all sigular values to be identical at low and high frequencies so that all crossover frequencies are approximately the same. This will result in all loops of the closed-loop system to have about the same speed of response. The details of the LQG/LTR design methodology are summarized in Refs [15,16].

5. EXAMPLE MANEUVER

The example combined maneuver chosen for simulation purpose is shown in Fig. 3. The end point is required to

move from point A to point B along a straight line for a travel of 0.4 m in 0.5 s (unconstrained maneuver), then move from point B to point C along a straight line for a travel of 1.32 m in 1.2 s and at the same time exert a force of 9.8 N on the constraint surface (constrained maneuver), and then finally move from point C to point D along a straight line for a travel of 0.4 m in 0.5 s (unconstrained maneuver). A fifth-order polynomial was used to interpolate the unconstrained segments so that the end-point of the manipulator starts and stops with zero acceleration. The desired force is slowly increased from 0 N to 9.8 N in the first 0.15 s of the constrained segment. Likewise, the force is slowly decreased from 9.8 N to 0 in the final 0.15 s of the constrained segment. A fifth-order polynomial is selected to interpolate the desired force trajectory for the acceleration and deceleration periods to provide for smooth transition. A constant tip velocity of 1.27 m/s with an acceleration period of 0.15 s at the beginning and a deceleration period of 0.15 s at the end was selected for motion in the y direction for the constrained segment. A fifth-order polynomial was again used to interpolate the acceleration and deceleration periods, which were provided so that the required motion can be accomplished in a smooth fashion. Polynomial interpolation is used rather than a constant velocity profile for the unconstrained segments because it results in less motion-induced vibration. This is desirable as Maples [1] has shown that a low impact velocity is helpful in reducing the problem of the end-point from bouncing during touchdown.

6. SIMULATED RESULTS

The system parameters of the flexible manipulator chosen in this study are similar to those used by Bayo [17]. The only difference is that a higher payload is considered here to increase the flexibility effects. The system parameters are $l_1 = l_2 = 0.66$ m, $m_1 = 0.3284$ kg/m, $m_2 = 0.1586$ kg/m, $M_1 = 1.049$ kg, $M_2 = 0.15$ kg, $I_{h1} = 0.00118$ kg-m^2, $I_{h2} = 0.00048$ kg-m^2, $EI_1 = 16.2563$ N/m^2, $EI_2 = 1.831$ N/M^2, and the stiffness of the force sensor is assumed to be 10,000 N/m.

The system matrices are time varying. Therefore, for the example combination maneuver, LQG/LTR compensators were designed using the linearized equations of motion (6) at three set points along the desired trajectory. The three set points chosen were at t=0.2 s, 0.9 s and 1.9 s. Note that the first and third set points are in the unconstrained segments of the maneuver, and the second set point is in the constrained segment of the maneuver.

The figure 4 shows the singular values of the recovered loop transfer function at the first set point (t=0.2). The minimum and maximum crossover frequencies obtained were about 17 and 20 rad/s, respectively. The design parameters chosen to meet the desired performance and robustness requirements for the first set point were $\mu = 2.0 \times 10^{-3}$ and $\rho = 1.0 \times 10^{-14}$, and the design matrix L was chosen so that the target feedback loop has identical singular values at both low and high frequencies. The LQG/LTR design parameters chosen for the second set point are $\mu = 2.5 \times 10^{-3}$ and $\rho = 1.0 \times 10^{-14}$. These parameters for the third set point are the same as those for the first set point. Note that the output variables to be controlled during the constrained segment have different physical units. Therefore, they were scaled so that they can be compared accurately. The output variables were scaled so that a 1 m error in position along the constraint surface is 200 times more serious than a 1 N error in force applied. The singular value plots for the second and third set points are similar to those obtained for the first set point.

Simulated response of the flexible manipulator are shown in Figures 5-12. The nonlinear equations of motion (1) were used to simulate the response of the manipulator. Figure 5 shows the time history of the force exerted on the constraint surface. When the end-point makes contact with the constraint surface, an impact force of about 1.5 N is generated. The force immediately decreases, but quickly follows the desired profile. Note that after impact, the force does not decrease to zero. In other words, once contact is made, the end-point will remain in contact with the constraint surface. A small initial value of 0.5 N was provided for the desired force profile so that the end-point would not break contact with the constraint surface on rebound. During the final phase of the constrained segment, the end-point bounces once, but the impact generated is small, less than 1 N. Figure 5 shows that the force is maintained within ± 1.4 N, which is equivalent to a displacement of ± 0.14 mm of the end-point. The coefficient of restitution was assumed to be zero in this study.

The position error in the x and y direction for the entire maneuver is minimal, as shown in Figures 6 and 7, respectively. Figure 8 shows the end-point velocity in x and y directions. Although not clearly visible, discontinuity in the velocity in the x direction exists when impact occurs. Figure 9 shows the tip deformation of both the links. When the end-point makes contact with the constraint surface and the force exerted is slowly increased, the outer link deforms a significant amount. But the magnitude decreases as the maneuver progresses. Similarly, during the deceleration phase of the constrained segment, the outer link deforms but not to the same extent as before. The modes excited during this deceleration phase are moderately damped during the unconstrained segment from point C to point D. As anticipated, the inner link deforms less compared to the outer link. Figure 10 shows the feedforward torques and the time history of the feedback torques is shown in Figs. 11 and 12. The contribution of the bending modes can be clearly seen in the time history of the feedback torques.

7. CONCLUDING REMARKS

The LQG/LTR compensator designed using the linearized equations of motion in Cartesian space operates on Cartesian space trajectory errors. It should be pointed out that a LQG/LTR compensator that operates on Cartesian space trajectory errors can be designed using the linearized equations of motion in joint space (2). This can be accomplished by appropriately defining the C matrix in the output equation. The linearized equations of motion in Cartesian space are developed in this study for two reasons. Firt, to choose the design matrix L such that the singular values of the target feedback loop are identical at both low and high frequencies, the inverse of the state matrix A must exist. This is not the case with the linearized equations of motion in joint space for unconstrained maneuvers. Second, the equations can be used

to develop a different Cartesian-based control system.

To implement the control system, the position of the end-point in Cartesian space and the force exerted by the manipulator on the constraint surface need to be measured. These requirements do not pose any difficulty, however. The force exerted by the manipulator can be measured by using a force sensor. The end-point position can be measured directly by using a vision system or indirectly by measureing the joint angles, and link deformations and slopes. Furthermore, joint angles can be measured by position encoders, link deflections by strain gauges, optical devices, or integrating accelermeter signals, and link slopes by optical devices.

The results presented show that the stability is maintained throught the example combined maneuver. If the force controller becomes unstable due to large impact forces at touchdown, it might be necessary to design a separate impact controller. In this case, control would be switched from position to impact control on touchdown, and from impact to force control after the impact has been dissipated.

REFERENCES

[1] J. A. Maples, "Force control of robotic manipulators with structural flexibility," Ph.D. Dissertation, Dept. of Electrical Eng., Stanford University, 1985.

[2] S. W. Tilley and R. H. Cannon, Jr., "Experiments on end-point position and force control of a flexible arm with a fast wrist," AIAA Guidance, Navigation and Control Conf., pp. 41-49, 1986.

[3] S. W. Tilley, R. H. Cannon, Jr. and R. Kraft, "End point force control of a very flexible manipulator with a fast end effector," Robotics: Theory and Applications, F. W. Paul and K. Youcef-Touni, eds., DSC-Vol. 3, ASME Winter Annual Meeting, pp. 1-9, 1986.

[4] G. W. Fan and I. A. Castelazo, "Force control in flexible manipulators," Proc. of the USA-Japan Symposium on Flexible Automation, pp. 361-368, 1988.

[5] F. Matsuno, Y. Sakawa and T. Asano, "Quasi-static hybrid position/force control of a flexible manipulator," Proc. of the IEEE Int. Conf. on Robotics and Automation, pp. 2838-2843, 1991.

[6] B. C. Chiou and M. Shahinpoor, "The effects of joint and flexibilities on the dynamic stability of force-controlled manipulators," Proc. of the IEEE Int. Conf. on Robotics and Automation, pp. 398-403, 1989.

[7] B. C. Chiou and M. Shahinpoor, "Dynamic stability analysis of a two-link force-controlled flexible manipulator," ASME J. of Dynamics Systems, Measurement, and Control, Vol. 112, pp. 661-666, December 1990.

[8] B. C. Chiou and M. Shahinpoor, "Experimental and theoretical observations on the dynamic stability of a one-link force-controlled flexible manipulators," Proc. of the IEEE Int. Conf. on Robotics and Automation, pp. 1208-1213, 1991.

[9] S. D. Eppiger and W. P. Seering, "On dynamic models of robot force control," Proc. of the IEEE Int. Conf. on Robotics and Automation, pp. 29-34, 1986.

[10] F. G. Pfeiffer, "Path and force control of elastic manipulators," Proc. of the IEEE Conf. on Decision and Control, pp. 514-519, December 1990.

[11] K. Richter and F. G. Pfeiffer, "A flexible link manipulator as a force measuring and controlling unit," Proc. of the IEEE Int. Conf. on Robotics and Automation, pp. 1212-1219, 1991.

[12] D. E. Whitney, "Historical perspective and state of the art in robot force control," Proc. of the IEEE Int. Conf. on Robotics and Automation, pp. 262-268, 1985.

[13] B. O. Choi, "Dynamic modeling Issues for contact tasks of flexible robotic manipulators," Proc. of the KSPE Spring Annual Meeting '93 pp. 175-180, 1993.

[14] L. S. Ward, "Dynamic and control of a nonlinear flexible manipulator," M.S Thesis, Dept. of Aeronautics and Astronautics, MIT, September 1986.

[15] J. C. Doyle and G. Stein, "Mutivariable feedback design: concepts for a classical/modern synthesis," IEEE Trans. on Automatic Control, Vol. AC-26, pp. 4-16, 1981.

[16] M. Athan, "A tutorial on the LQG/LTR method," Proc. of American Control Conf., pp. 1287-1296, 1986.

[17] M. Bayo, "Computed torque for the position control of open-chain flexible robots," Proc. of the Int. Conf. on Robotics and Automation, pp. 316-321, 1988.

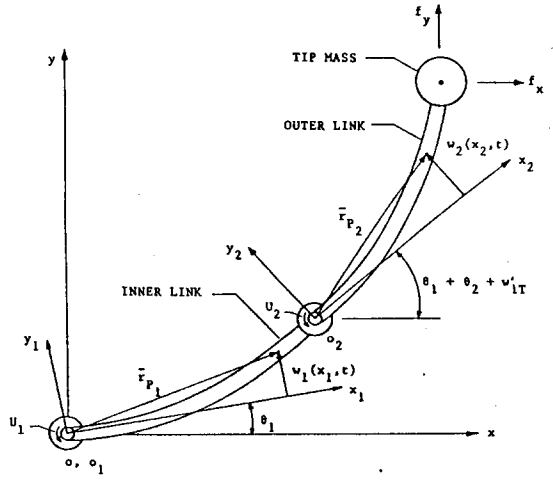

Fig. 1 Schematic of a Planar Two-Link Flexible Manipulator

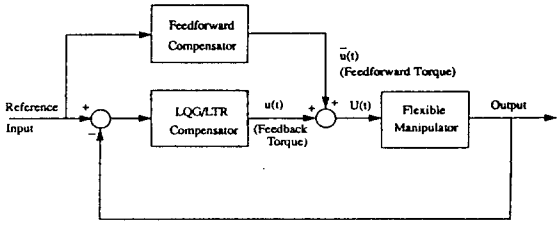

Fig. 2 Block Diagram of the Control System

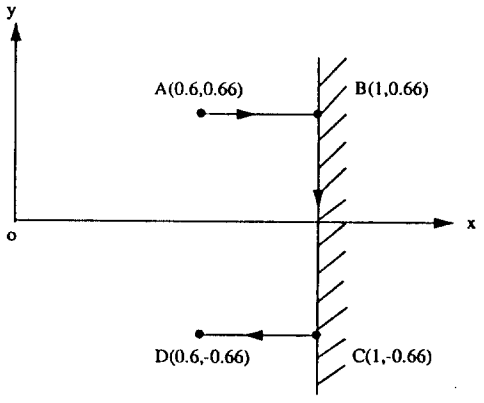

Fig. 3 Combined Maneuver for Position/Force Control Simulation

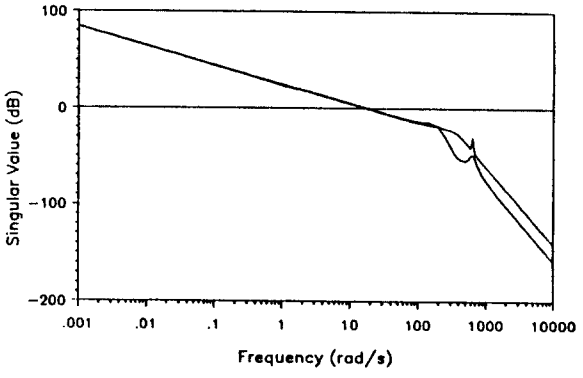

Fig. 4 Singular Values of the LQG/LTR Loop Transfer Function

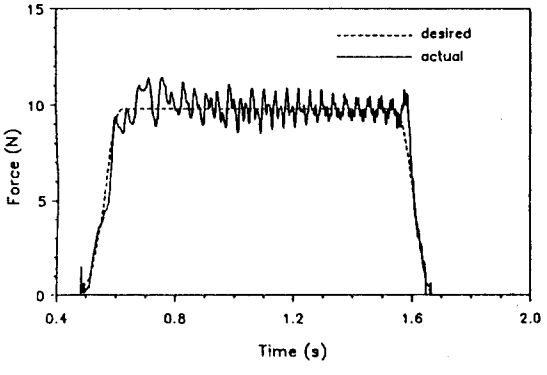

Fig. 5 Time History of Force Exerted on the Constraint Surface

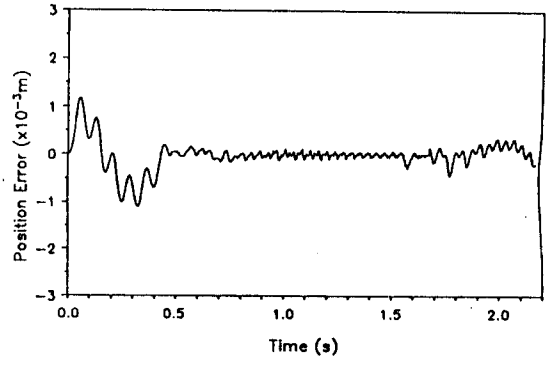

Fig. 6 Time History of the Position Error in x Direction

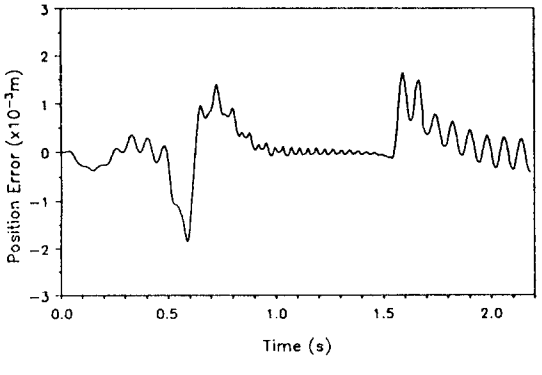

Fig. 7 Time History of the Position Error in y Direction

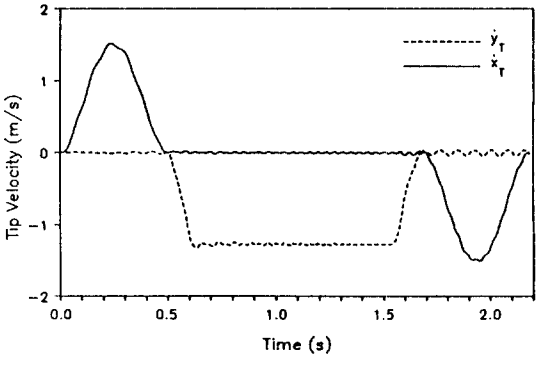

Fig. 8 Time History of the End-point Velocities

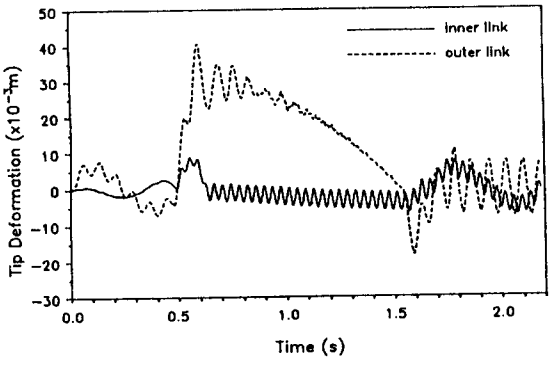

Fig. 9 Tip Deformation of Manipulator Links

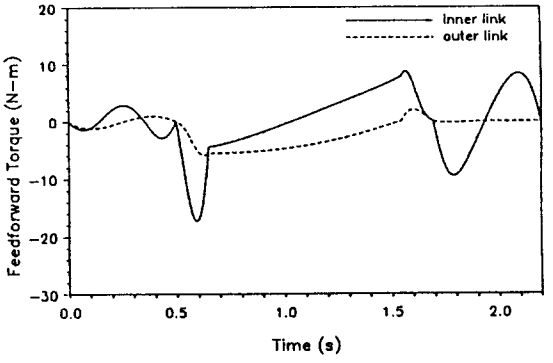

Fig. 10 Time History of Feedforward Torques

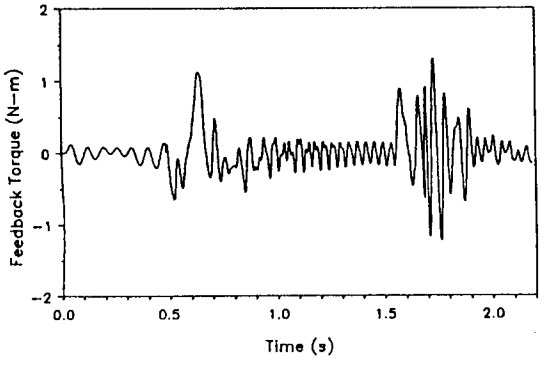

Fig. 11 Time History of feedback Torque for Inner Link

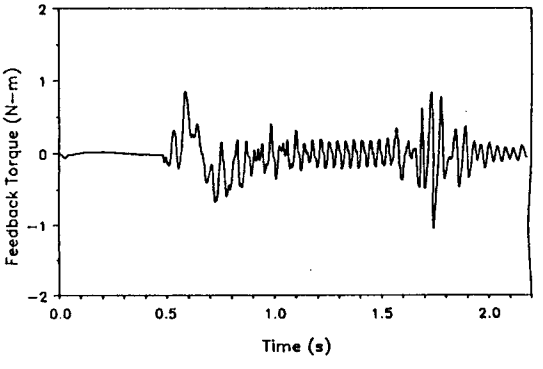

Fig. 12 Time History of feedback Torque for Outer Link